Proceedings of the ASME 2024 19th International Manufacturing Science and Engineering Conference
MSEC2024
June 17-21, 2024, Knoxville, Tennessee

MSEC2024-125241

TOWARD RAPID PROCESS QUALIFICATION OF LASER POWDER BED FUSION: MODEL PREDICTIVE CONTROL OF PART THERMAL HISTORY

Alexander Riensche
Virginia Tech
Blacksburg, VA

Benjamin Bevans
Virginia Tech
Blacksburg, VA

John Sions
CCAM
Disputanta, VA

Kyle Snyder
CCAM
Disputanta, VA

Yuri Plotnikov
CCAM
Disputanta, VA

Derek Hass
CCAM
Disputanta, VA

Prahalada Rao
Virginia Tech
Blacksburg, VA

ABSTRACT

This work pertains to the laser powder bed fusion (LPBF) additive manufacturing process. The goal of this work is to mitigate the expense and time required for qualification of laser powder bed fusion processed parts. In pursuit of this goal, the objective of this work is to develop and apply a physics-based model predictive control strategy to modulate the thermal history before the part is built. The key idea is to determine a desired thermal history for a given part a priori to printing using a physics-based model. Subsequently, a model predictive control strategy is developed to attain the desired thermal history by changing the laser power layer-by-layer. This is an important area of research because the spatiotemporal distribution of temperature within the part (also known as the thermal history) influences flaw formation, microstructure evolution, and surface/geometric integrity, all of which ultimately determine the mechanical properties of the part. Currently, laser powder bed fusion parts are qualified using a build-and-test approach wherein parameters are optimized by printing simple test coupons, followed by examining their properties via materials characterization and testing – a cumbersome and expensive process that often takes years. These parameters, once optimized, are maintained constant throughout the process for a part. However, thermal history is a function of over 50 processing parameters including material properties and part design, consequently, the current approach of parameter optimization based on empirical testing of simple test coupons seldom transfers successfully to complex, practical parts. Rather than instinctive process parameter optimization, the model predictive control strategy presents a radically different approach to LPBF part qualification that is based on understanding and modulating the causal thermal physics of the process. The approach has three steps: (Step 1) Predict – given a part geometry, use a rapid, mesh-less physics-based simulation model to predict its thermal history, analyze the predicted thermal history trend, isolate potential red flag problems such as heat buildup, and set a desired thermal history that corrects deleterious trends. (Step 2) Parse – iteratively simulate the thermal history as a function of various laser power levels layer-by-layer over a fixed time horizon. (Step 3) Select – the laser power that provides the closest match to the desired thermal history. Repeat Steps 2 and 3 until the part is completely built. We demonstrate through experiments with various geometries two advantages of this model predictive control strategy when applied to laser powder bed fusion: (i) prevent part failures due to overheating and distortion, while mitigating the need for anchoring supports; and (ii) improve surface integrity of hard to access internal surfaces.

Keywords: Laser Powder Bed Fusion, Process Control, Thermal Modeling, Support Elimination

1. INTRODUCTION

Laser powder bed fusion (LPBF, FIGURE 1) is an additive manufacturing (AM) process in which layers of metal powder are raked on a build plate, and selectively melted using a high power infrared laser [1]. The LPBF process has emerged as a favorable method to create novel and advanced geometry which is impossible to create with traditional manufacturing techniques. The technology is also attractive due to its ability to

reduce lead times and assembly part count, simplifying the manufacturing process [2-4].

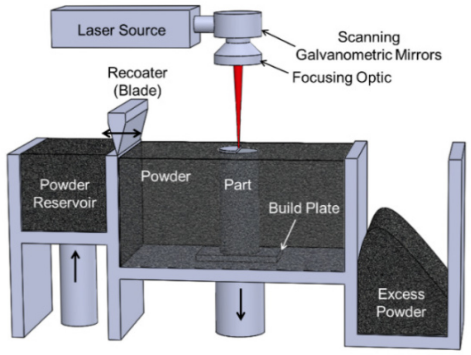

FIGURE 1: SCHEMATIC OF THE LASER POWDER BED FUSION PROCESS (LPBF).

Despite the promise of LPBF, and AM in general, technology adoption has been limited by the tendency of the processes to form flaws such as porosity, cracking, and inconsistent microstructure [5, 6]. These flaws in LPBF are primarily driven by the temperature distribution in the part caused by the local melting by the laser, as well as the global heat accumulation[7]. Currently, in LPBF parameters are selected empirically based on building simple calibration coupons. Unfortunately, such empirical parameter optimization does not transfer to complex geometries as each part shape has a unique temperature distribution [8]. This leads to a cumbersome and expensive build-and-test qualification process for every new part design which is not practical for industry application. Moreover, such optimized part parameters remain fixed throughout the part irrespective of layer-wise changes in the cross-section.

The objective of this work is to create a framework in which the layer-by-layer thermal distribution, commonly known as thermal history, for each part geometry is optimized and controlled. This is a radical departure from the status quo of optimizing the processing parameters for a sample coupon and maintaining the settings fixed irrespective of the geometry. To accomplish this objective, we propose a three-step model predictive control approach as summarized in FIGURE 2. We note that these steps are completed autonomously with minimal human intervention.

Step 1 Predict – given a part geometry and build layout, we first use a rapid, mesh-less physics-based simulation mode to predict its thermal history [9]. These predictions represent the uncontrolled thermal history. We note deleterious trends from the uncontrolled thermal history, and consequently, determine the target (T_{ideal}) without such flaws.

Step 2 Parse – We iteratively simulate the thermal history as a function of various laser power levels layer-by-layer over a fixed space horizon of 5 model layers (~25 actual layers, 0.5 mm height).

Step 3 Select – The laser power that provides the closest match to the desired thermal history T_{ideal} in terms of the mean absolute deviation is ascertained and selected. We note that, upper and lower limits are placed on the laser power.

Steps 2 and 3 are repeated until the part is completely built. Taken together these steps solve the inverse problem, i.e., they determine the optimal laser power to obtain T_{ideal}.

This model-based control approach can be used for various purposes including: process parameter optimization, avoiding build failures, mitigating support structures, and reducing flaw formation. For example, in FIGURE 2, we applied the approach to eliminate supports in a relatively complex arch-shaped part. Such parts are difficult, if not impossible, to build owing to heat accumulation in the overhang arch section. This heat buildup often causes thermal-induced distortion and build failures due to recoater contact. The support structure prevents distortion; however, they require considerable and precise post-process machining to remove, resulting in increased material waste. Adaptively changing parameters also minimizes energy waste, further reducing production costs.

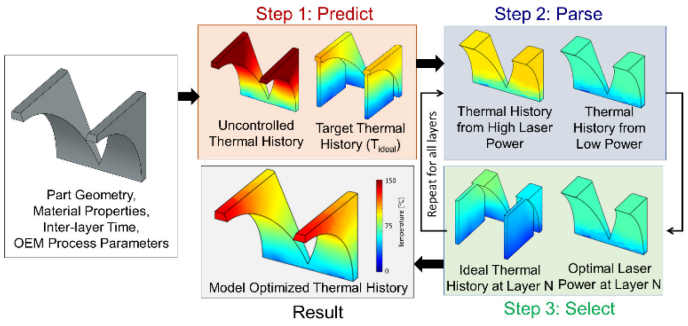

FIGURE 2: SUMMARY OF THE MODEL PREDICTIVE CONTROL FRAMEWORK. THE KEY IDEA IS TO USE RAPID, PART LEVEL SIMULATIONS IN A MODEL PREDICTIVE CONTROL FRAMEWORK TO MATCH AN IDEAL THERMAL HISTORY.

2. MATERIALS AND METHODS

2.1 Experimental Setup

In this work, 10 Stainless Steel 316L parts consisting of four unique geometries were created on an EOS M290 LPBF system at the Commonwealth Center for Advanced Manufacturing, Disputanta, VA. A picture of the setup is shown in FIGURE 3(a). The final build plate and geometry details are shown in FIGURE 4. In this paper, we discuss results from the arch-shaped bridge and bell crank geometries. The parts varied in size and height from 25 mm (bridge) to 42 mm tall (bell crank). The bridge part required 1250 layers and the bell crank required 2100 layers at a layer thickness of 20 µm, and laser velocity of 1083 $mm \cdot s^{-1}$. In all, the build required 12 hours to complete.

One of the two bridge parts was built with supports under fixed (nominal) parameters, and the other without supports with layer-by-layer laser power changes identified by the model-predictive control strategy presented in this work, and discussed briefly in the context of FIGURE 2. Likewise, one of the bell crank parts was created with manufacturer-recommended nominal process parameters and the other was built using the model-predictive control strategy discussed in Sec. 2.2. Nominal

process parameters are recommended by the machine tool manufacturer (EOS) and are summarized in FIGURE 4.

Laser power was varied for the controlled processing parameters, with minimum and maximum laser power settings determined by cases studies in literature that showed significant lack-of-fusion porosity formation below 50 J/mm^3, and key hole and gas porosity formation above 100 J/mm^3 [10]. Hence, the limits of the laser power adjustment were limited to values between 145 W to 225 W.

After creation, the parts were examined with X-Ray computed tomography (XCT) on a North Star Imaging system with a 15µm voxel resolution. No porosity was detected in any of the parts printed in this work. For the bell crank geometry, the surface roughness was also tested on the exterior of all parts. In our future work, these and other parts on the build plate will be cross sectioned and their microstructure will be characterized using optical and scanning electron microscopy.

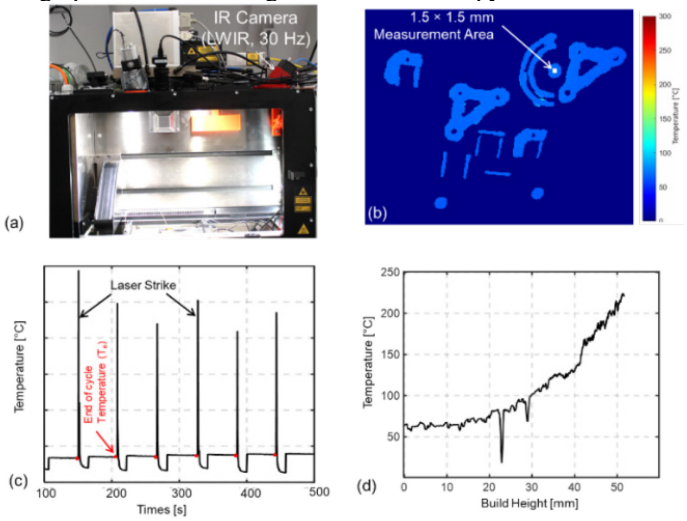

FIGURE 3: (a) MACHINE SETUP WITH INFRARED CAMERA (b) END-OF-CYCLE TEMPERATURE EXTRACTION METHODOLGY. REGIONS OF INTEREST ARE SELECTED FOR EACH PART BY TAKING THE LOWEST TEMPERATURE AT EACH LAYER (c), END-OF-CYCLE TEMPERATURE CAN BE EXTRACTED (d).

During the build, thermal trends were monitored with a long wave infrared (IR) camera. The data from the IR camera is necessary to validate the thermal model. The camera was calibrated with a method similar to our previous works to ensure accurate surface temperature measurements were taken [9]. End-of-cycle temperature was extracted according to the method shown in FIGURE 3.

End-of-cycle temperature describes how heat accumulates on the top surface of parts and has been shown in our previous works to correlate to flaws such as porosity, distortion, and geometric deviation [9, 11].

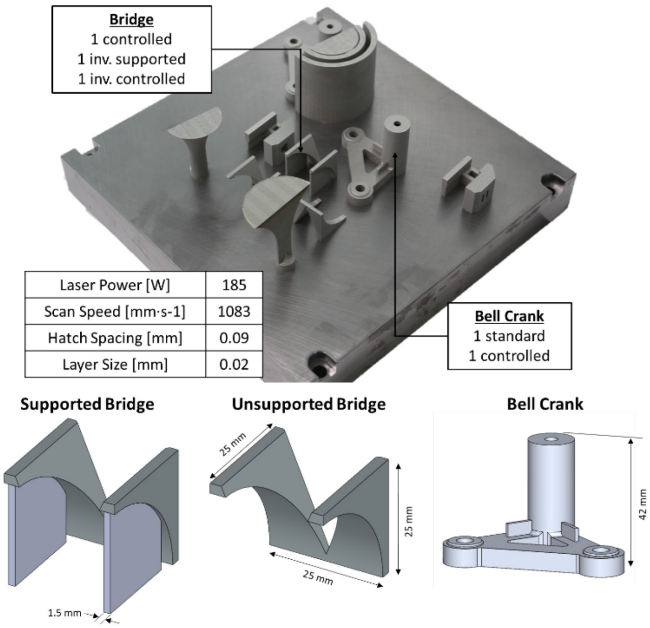

FIGURE 4: (a) BUILD PLATE WITH NOMINAL PROCESS PARAMETERS USED TO DEMONSTRATE THE MODEL PREDICTIVE CONTROL FRAMEWORK PROPOSED IN THIS WORK. (b) SUMMARY OF GEOMETRIES WITH DIMENSIONS CREATED IN THIS WORK.

The procedure to obtain the end-of-cycle temperature is as follows. A region of interest is selected for each part (FIGURE 3b), and the temperature of this region is tracked for all of the time domain, across multiple layers. (FIGURE 3c). The temperature immediately before the subsequent laser strike for the next layer is extracted as the temperature for the current layer. This results in a thermal profile as a function of build height (FIGURE 3d).

2.2 Model Predictive Control

To implement model predictive control in LPBF, a rapid thermal modeling approach is required, as multiple process parameters are tested at each layer. In other words, a model that is accessible for solving the inverse problem is essential for the approach to succeed. Traditional thermal modeling approaches using finite element (FE) methods are too slow for this application due to the computationally expensive and memory intensive remeshing step. Commercial LPBF simulation software do not allow for such autonomous changes. As such, this work uses the graph theory thermal modeling approach pioneered in the author's previous works [9, 12]. Briefly summarized, the graph theory model solves the heat diffusion equation for each point (x,y,z) at every sampled point in time (t). This relationship is defined in Eqn. (1).

$$\rho c_p \frac{\partial T(x,y,z,t)}{\partial t} - k \overbrace{\left(\frac{\partial^2}{\partial x^2} + \frac{\partial^2}{\partial y^2} + \frac{\partial^2}{\partial z^2}\right)}^{Laplacian\ operator} T(x,y,z,t) = Q \quad (1)$$

In Eqn. (1), ρ is the material density [kg·m^{-3}], c_p is the specific heat [J·kg^{-1} ·K^{-1}], and k is the conductivity [J·s^{-1} ·m^{-1}·K^{-1}], and Q is the rate of heat supplied per unit volume of material melted [J·s^{-1}·m^{-3}], called volumetric heat flux. Material properties are assumed to be fixed and are measured at 250°C. The term Q is a function of the processing parameters: laser power (P, [W]), laser velocity (V, [m·s^{-1}]), hatch spacing (H, [m]), layer height (L, [m]), and time when the laser is active (t, [s]); $\mathrm{Q} = \frac{\mathrm{P}}{\mathrm{V}\cdot\mathrm{H}\cdot\mathrm{L}\cdot t}$.

The graph theory thermal model replaces the continuous Laplacian operator $\left(\frac{\partial^2}{\partial x^2}+\frac{\partial^2}{\partial y^2}+\frac{\partial^2}{\partial z^2}\right)$ in the previous equation with a space-representative discrete Laplacian matrix (L). By substituting the Laplacian, simplifying, and solving the differential equation, the following solution can be obtained.

$$\mathrm{T}(x,y,z,\mathrm{t}) = \phi e^{-\frac{k}{\rho c_p}\Lambda t}\phi'\left(\frac{\mathrm{A_e S_l}}{\rho v c_p}\frac{\mathrm{P}}{\mathrm{V}} + \mathrm{T_{prev}}\right) \quad (2)$$

Here, the thermal history $\mathrm{T}(x,y,z,\mathrm{t})$ is solved as a function of the eigenvalues (Λ), eigenvectors (ϕ), and time (t) of the Laplacian matrix (L). $\mathrm{A_e}$ is the effective laser absorptivity, $\mathrm{S_l}$ length scanned per layer (a function of hatch spacing, [mm]), P [W] laser power, V [mm·s^{-1}] laser velocity, v [mm^3] volume of material melted in a layer (a product of scanned area and layer height), and $\mathrm{T_{prev}}$ [°C] is the temperature of the previous layer (from simulation). In this work, $\mathrm{A_e} = 0.60$ based on experiments by Ye *et al.* at Lawrence Livermore National Laboratory [13]. In Eqn. (2), the part geometry and time are completely decoupled from the applied laser heating condition. This allows multiple process parameters to be tested without significant computation overhead, which is necessary for the implementation of a model predictive control scheme for LPBF.

Model predictive control enables process modeling to control system properties. This technique is especially useful where the system is complex or the system lacks feedback mechanisms which would enable the use of feedback control systems [14]. In this work, a simple iterative control scheme was selected to control the thermal history. The control scheme used in this work was first summarized in FIGURE 2. Herewith we augment the summary with critical details.

In Step 1(Predict), an ideal thermal history $\mathrm{T_{ideal}}$ for the entire part is identified. For this purpose, the thermal history is predicted for the part geometry under fixed processing conditions suggested by the manufacturer. These thermal simulations required less than 20 minutes to complete for each geometry. This so-called uncontrolled or original thermal history is denoted as $\mathrm{T_{original}}$. Next, in Step 1, deleterious trends, such as heat buildup are identified by analyzing $\mathrm{T_{original}}$. Lastly, these undesirable trends in $\mathrm{T_{original}}$ are negated (corrected) by proposing an ideal trend $\mathrm{T_{ideal}}$. The identification of an appropriated $\mathrm{T_{ideal}}$ is the human-in-the-loop step.

In Step 2 (Parse), considering layer N, the effect of several possible laser power settings are simulated with five layers of lookahead (N+5). In other words, the prediction horizon is 5 layers. We note that the thermal simulation implements a meta-layer approach where multiple layers are considered to be deposited at once. This simplification is inherent to most FE-based commercial software. In this work 5 actual layers (100 μm) correspond to 1 model layer. Hence, the lookahead corresponds to 0.5 mm of actual build height.

Lookahead of the simulation time horizon is used to prevent oscillations around the optimal solution. Longer time horizons excessively burden computation time, reducing the benefit of the approach. The graph theory model, as in commercial approaches, defines a layer as 5 actual layers, i.e., 100 μm layers. Five levels of laser power were analyzed: θ_1 = 146 W, θ_2 =156 W, θ_3 = 176 W, θ_4 = 195 W, and θ_5 = 225 W.

In Step 3 (Select), after the thermal history $\mathrm{T_P}(\theta_i)$, i = {1...5} from each of the five laser power levels are simulated, we select the optimal laser power θ_* corresponding thermal history $\mathrm{T_P}(\theta_i)$ which results in the minimum mean absolute deviation (MAD) from the ideal thermal history $\mathrm{T_{ideal}}$. Steps 2 and 3 are repeated after every two simulated layers. Hence, this model predictive control approach overwrites three topmost thermal history meta layers with new parameters every iteration. The end result is a laser power plan determined at 100 μm steps for the entire part. Because the approach self-enforces laser power between 146W and 225W, it inherently avoids lack-of-fusion and keyhole porosity [10].

The model predictive control scheme was able to complete and identify the optimal laser power θ_* for each layer in approximately three hours for each geometry which was created. In our previous work, we have observed defects at the interface of layers where large process parameter changes occur [15]. Therefore, to reduce the severity of the process parameter changes a 15-point moving average applied to the laser power plan generated by the controller. Because the optimal laser power settings θ_* must be programmed into the LPBF machine by the operators manually, the parameter set was further simplified by averaging laser power recommendations every 4 mm of build height. Simulation studies showed minimal differences between the end-of-cycle temperature for the as-predicted and smoothed laser power estimates.

3. RESULTS AND DISCUSSION

3.1 Bridge

This result demonstrates the utility of the model predictive control approach for eliminating support structures in LPBF parts. The end-of-cycle temperature predicted by the model for the supported uncontrolled bridge and unsupported controlled bridge geometries are shown in FIGURE 5. The aim of the controller was to adjust the laser power layer-by-layer for the unsupported bridge such that its thermal history would match that of the supported bridge. In other words, the $\mathrm{T_{ideal}}$ is the thermal history of the supported bridge shown in FIGURE 5(left). Also, in FIGURE 5, the model predictions are overlaid on observed end-of-cycle temperature acquired from the IR thermal camera.

The model predictions match the IR data with symmetric mean absolute error (SMAPE) less-than 10%. We note that the model parameters were calibrated against a different part from the build plate shown in FIGURE 4 and not discussed in this

work for brevity. This affirms that the graph theory model accurately predicts the effect of part shape and process parameter changes applied to the part. The end-of-cycle temperature and laser power changes for the unsupported bridge parts is shown in FIGURE 5(right). These optimized conditions were obtained autonomously within 3 hours.

Shown in FIGURE 6 are the thermal histories for three parts. In FIGURE 6(left) is the thermal simulation for the unsupported and uncontrolled bridge. This part is not manufactured due to high chance of build failure from recoater crash. In FIGURE 6(middle) is the uncontrolled supported bridge, which is the T_{ideal}. This was selected as the target temperature as it was hypothesized that the matching thermal history of the supported part would allow the unsupported geometry to succeed. In FIGURE 6(right) is the unsupported controlled bridge-shaped part built with the model predictive control strategy. The model predictive control strategy successfully eliminated the need for support by reducing the heat build-up in the overhang section.

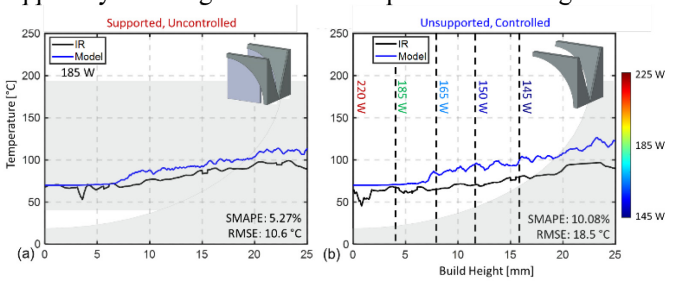

FIGURE 5: END-OF-CYCLE TEMPERATURE COMPARISIONS TO IR DATA FOR THE SUPPORTED UNCONTROLLED BRIDGE (a) AND (b) UNSUPPORTED CONTROLLED BRIDGE. THE LASER POWER MODULATED LAYER-BY-LAYER IS SHOWN.

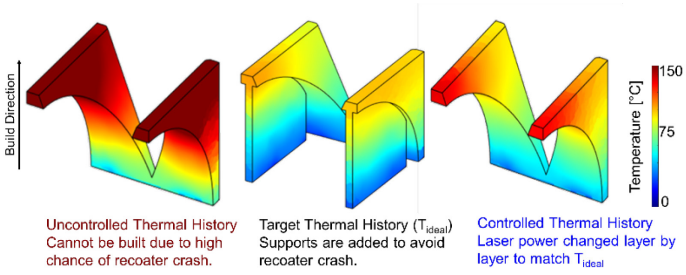

FIGURE 6: END-OF-CYCLE TEMPERATURE COMPARISIONS FOR THE UNSUPPORTED UNCONTROLLED BRIDGE, SUPPORTED UNCONTROLLED BRIDGE (TARGET THERMAL HISTORY), AND UNSUPPORTED CONTROLLED PARTS

FIGURE 7 shows an XCT slice in the X-Z plane for the supported uncontrolled, and unsupported controlled bridges. Given the extreme nature of this geometry, distortion was observed in both parts at ~22 mm of build height to an identical degree. This indicates that the model predictive control strategy used in this work does not degrade the part quality.

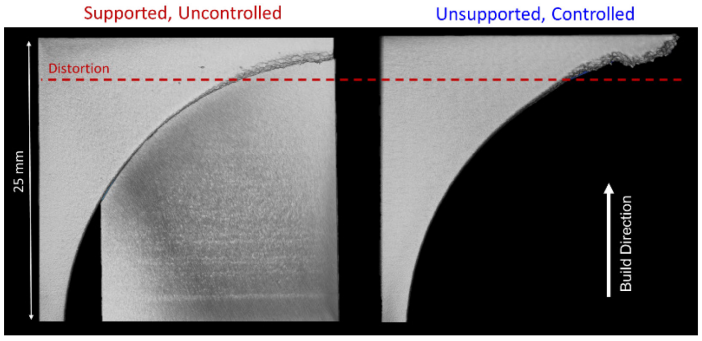

FIGURE 7: XCT COMPARISION BETWEEN THE UNCONTROLLED SUPPORTED (LEFT) AND CONTROLELED UNSUPPORTED BRIDGES (RIGHT). PROCESS CONTROL ALLOWED THE PART TO BE MADE WITHOUT SUPPORT MATERIAL WITH EQUIVILANT DISTORTION.

3.2 Bell Crank

Three thermal histories for the bell crank geometry are reported in FIGURE 8. The thermal history ($T_{original}$) for the uncontrolled bell crank built at a fixed laser power of 195 W tends to accumulate heat as it grows due to the poor thermal conductivity of the metal powder. A visual depiction of the thermal history for the uncontrolled bell crank is shown in FIGURE 9. In FIGURE 8, heat buildup beyond the 9 mm build height is observed in the case of the uncontrolled bell crank demarcated by the red line. A desirable or ideal thermal trend T_{ideal} would be to avoid the heat buildup and maintain a constant end-of-cycle temperature throughout the part as noted with the black line in FIGURE 8.

In other words, the control target (T_{ideal}) was to maintain a constant end-of-cycle temperature after 9 mm of build height. The thermal history obtained by applying the model predictive control strategy is demarcated with the blue line in in FIGURE 8. The model predictive control approach successfully reduced the heat accumulation in the part as visually evident in FIGURE 9 (right) by altering the laser power in a layer-wise manner. The achieved surface temperature does not match the T_{ideal} because, the laser power is constrained between 145 W and 225 W. Use of model predictive control reduced the symmetric mean absolute percentage error (SMAPE) from T_{ideal} from 10.6% to 7.6%. This reduction in bulk temperature improved internal surface finish, as shown in FIGURE 10.

The laser power settings as a function of layer height recommended by the controller are noted in FIGURE 9 (right). The model predictive control approach converged to these laser power settings autonomously within 3 hours. We note that while heat buildup was minimized by the model predictive control, it was not completely eliminated. This is because, the laser power

cannot be reduced beyond 145 W so as to avoid porosity, which would be deleterious to part properties.

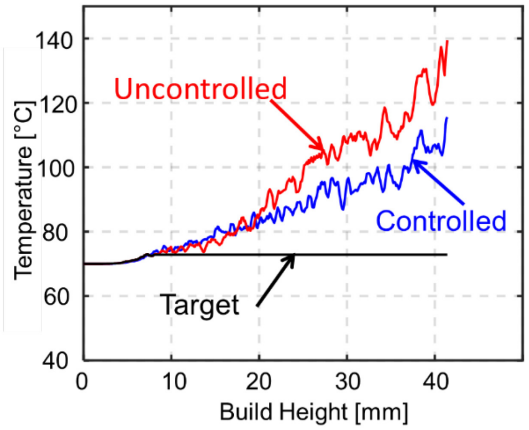

FIGURE 8: END-OF-CYCLE TEMPERATURE FOR THE STANDARD AND CONTROLLED CASES, AND THE TARGET TREND (T_{ideal}). PROCESS CONTROL WAS ABLE TO LIMIT HEAT ACCUMULATION IN THE PART.

From examining the internal surface of the bell crank with XCT, it was observed that the heat buildup in the uncontrolled bell crank resulted in a rougher surface on the internal bore. Three measurements were acquired with an optical profilometer of the measurable external surfaces of the bell crank confirmed the foregoing – the surface roughness for the external surface of the uncontrolled bell crank resulted in Sa ~ 14 µm, compared to Sa~ 12 µm for the controlled case. A small improvement in the surface roughness, as small as 2 µm has been shown to considerably improve the fatigue life [16].

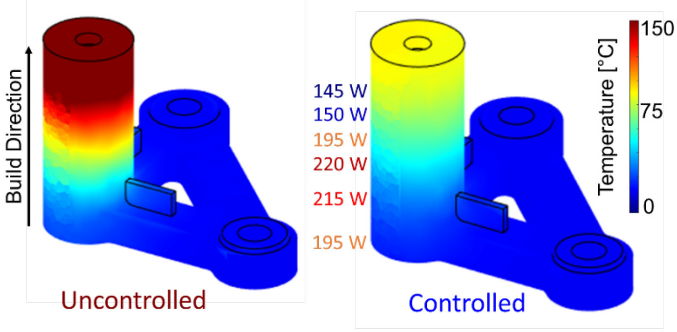

FIGURE 9: END-OF-CYCLE TEMPERATURE DISTRIBUTION FOR THE UNCONTROLLED (LEFT) AND CONTROLLED (RIGHT) BELL CRANK PARTS. NOTE THE HEAT BUILD-UP IN THE UNCONTROLLED BELL CRANK.

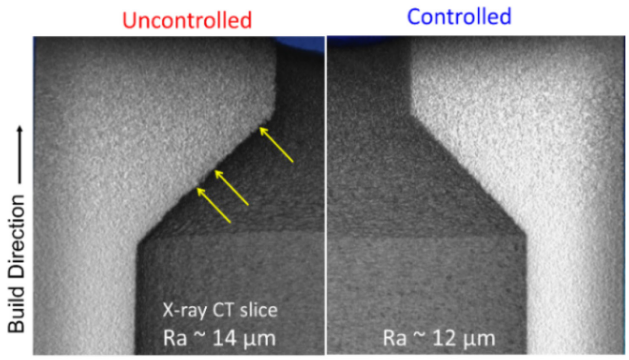

FIGURE 10: XCT AND SURFACE ROUGHNESS COMPARISON BETWEEN UNCONTROLLED (LEFT) AND CONTROLLED (RIGHT) BELL CRANK PARTS. MODEL PREDICTIVE CONTRO REDUCED SURFACE ROUGNESS OF INTERNAL AND EXTERNAL SURFACE WITHOUT AN INCREASE IN POROSITY.

4. CONCLUSION

We developed and implemented a model predictive control approach to reduce thermal-induced flaws in LPBF parts. In this approach laser power is automatically changed layer-by-layer based on information from a physics-based model to match an ideal thermal history. This work showed two scenarios where this approach could be useful in industry. First, the approach can reduce, if not eliminate, the need for support structures. It can thus mitigate the considerable expense associated with post-process removal of supports. The second scenario demonstrates that the approach can improve the surface finish of external and internal, hard to process features. In our future research, we will expand the model predictive control approach to obtain a desired microstructure.

ACKNOWLEDGEMENTS

Prahalada Rao acknowledges funding from the National Science Foundation (NSF) via Grant numbers: CMMI-2309483/1752069, OIA-1929172, PFI-TT 2322322/2044710, CMMI-1920245, ECCS-2020246, CMMI-1739696, and CMMI-1719388 for funding his research program.

REFERENCES

[1] Chowdhury, S., Yadaiah, N., Prakash, C., Ramakrishna, S., Dixit, S., Gupta, L. R., and Buddhi, D., 2022, "Laser powder bed fusion: a state-of-the-art review of the technology, materials, properties & defects, and numerical modelling," Journal of Materials Research and Technology, 20, pp. 2109-2172.

[2] Blakey-Milner, B., Gradl, P., Snedden, G., Brooks, M., Pitot, J., Lopez, E., Leary, M., Berto, F., and du Plessis, A., 2021, "Metal additive manufacturing in aerospace: A review," Materials & Design, 209, p. 110008.

[3] Gradl, P. R., Tinker, D. C., Ivester, J., Skinner, S. W., Teasley, T., and Bili, J. L., 2021, "Geometric feature reproducibility for laser powder bed fusion (L-PBF) additive manufacturing with Inconel 718," Additive Manufacturing, 47, p. 102305.

[4] Najmon, J. C., Raeisi, S., and Tovar, A., 2019, "2 - Review of additive manufacturing technologies and applications in the aerospace industry," Additive Manufacturing for the Aerospace Industry, F. Froes, and R. Boyer, eds., Elsevier, pp. 7-31.
[5] Mostafaei, A., Zhao, C., He, Y., Reza Ghiaasiaan, S., Shi, B., Shao, S., Shamsaei, N., Wu, Z., Kouraytem, N., Sun, T., Pauza, J., Gordon, J. V., Webler, B., Parab, N. D., Asherloo, M., Guo, Q., Chen, L., and Rollett, A. D., 2022, "Defects and anomalies in powder bed fusion metal additive manufacturing," Current Opinion in Solid State and Materials Science, 26(2), p. 100974.
[6] Snow, Z., Nassar, A. R., and Reutzel, E. W., 2020, "Invited Review Article: Review of the formation and impact of flaws in powder bed fusion additive manufacturing," Additive Manufacturing, 36, p. 101457.
[7] Oliveira, J. P., LaLonde, A. D., and Ma, J., 2020, "Processing parameters in laser powder bed fusion metal additive manufacturing," Materials & Design, 193, p. 108762.
[8] Narasimharaju, S. R., Zeng, W., See, T. L., Zhu, Z., Scott, P., Jiang, X., and Lou, S., 2022, "A comprehensive review on laser powder bed fusion of steels: Processing, microstructure, defects and control methods, mechanical properties, current challenges and future trends," Journal of Manufacturing Processes, 75, pp. 375-414.
[9] Riensche, A., Bevans, B. D., Smoqi, Z., Yavari, R., Krishnan, A., Gilligan, J., Piercy, N., Cole, K., and Rao, P., 2022, "Feedforward control of thermal history in laser powder bed fusion: Toward physics-based optimization of processing parameters," Materials & Design, 224, p. 111351.
[10] Gor, M., Soni, H., Wankhede, V., Sahlot, P., Grzelak, K., Szachgluchowicz, I., and Kluczyński, J., 2021, "A Critical Review on Effect of Process Parameters on Mechanical and Microstructural Properties of Powder-Bed Fusion Additive Manufacturing of SS316L," Materials.
[11] Yavari, R., Smoqi, Z., Riensche, A., Bevans, B., Kobir, H., Mendoza, H., Song, H., Cole, K., and Rao, P., 2021, "Part-scale thermal simulation of laser powder bed fusion using graph theory: Effect of thermal history on porosity, microstructure evolution, and recoater crash," Materials & Design, 204, p. 109685.
[12] Cole, K. D., Riensche, A., and Rao, P. K., 2022, "Discrete Green's functions and spectral graph theory for computationally efficient thermal modeling," International Journal of Heat and Mass Transfer, 183, p. 122112.
[13] Ye, J., Khairallah, S. A., Rubenchik, A. M., Crumb, M. F., Guss, G., Belak, J., and Matthews, M. J., 2019, "Energy Coupling Mechanisms and Scaling Behavior Associated with Laser Powder Bed Fusion Additive Manufacturing," Advanced Engineering Materials, 21(7), p. 1900185.
[14] Mayne, D. Q., 2014, "Model predictive control: Recent developments and future promise," Automatica, 50(12), pp. 2967-2986.
[15] Bevans, B., Barrett, C., Spears, T., Gaikwad, A., Riensche, A., Smoqi, Z., Halliday, H., and Rao, P., 2023, "Heterogeneous sensor data fusion for multiscale, shape agnostic flaw detection in laser powder bed fusion additive manufacturing," Virtual and Physical Prototyping, 18(1).
[16] Maleki, E., Bagherifard, S., and Guagliano, M., 2023, "Correlation of residual stress, hardness and surface roughness with crack initiation and fatigue strength of surface treated additive manufactured AlSi10Mg: Experimental and machine learning approaches," Journal of Materials Research and Technology, 24, pp. 3265-3283.